

Dielectric properties in heteroepitaxial $\text{Ba}_{0.6}\text{Sr}_{0.4}\text{TiO}_3$ thin films: Effect of internal stresses and dislocation-type defects

C. L. Canedy, Hao Li,^{a)} S. P. Alpay, L. Salamanca-Riba, A. L. Roytburd, and R. Ramesh
Department of Materials and Nuclear Engineering, University of Maryland, College Park, Maryland 20742

(Received 8 May 2000; accepted for publication 11 July 2000)

A series of heteroepitaxial $\text{Ba}_{0.6}\text{Sr}_{0.4}\text{TiO}_3$ were grown on $0.29(\text{LaAlO}_3):0.35(\text{Sr}_2\text{TaAlO}_6)$ substrates using pulsed-laser deposition. X-ray characterization revealed compressive in-plane stresses in the thinnest films, which were relaxed in a continuous fashion with increasing thickness. A theoretical treatment of the misfit strain was in good agreement with the measured out-of-plane lattice parameter. The low-frequency dielectric constant was measured to be significantly less than the bulk value and found to decrease rapidly for films less than 100 nm. A thermodynamic model was developed to understand the reduction in dielectric constant. By observing the microstructure using plan-view and cross-section transmission electron microscopy, we identified local strain associated with a threading dislocation density on the order of 10^{11} cm^{-2} as a possible mechanism for dielectric degradation in these films. © 2000 American Institute of Physics.
 [S0003-6951(00)00937-2]

Ferroelectric materials offer an enticing prospect for incorporation into frequency-agile microwave electronic components, including phase shifters, varactors, tunable filters, and antennas.¹⁻⁵ Ultimately, these materials are envisioned to enter into microwave integrated circuits for possible insertion in satellite and wireless communication platforms.^{1-3,6-8} In this area, $(\text{Ba,Sr})\text{TiO}_3$ -based ceramic thin films are considered by many as the forerunners for room-temperature (RT) applications.^{3,5-7,9,10} $(\text{Ba,Sr})\text{TiO}_3$ solid solutions exhibit a large permittivity that can be as large as 10 000 for bulk samples near the ferroelectric transition temperature (T_C). Tuning applications rely on the nonlinear dielectric response of ferroelectric materials, which can be significant close to T_C .¹¹

In this letter, we report on a systematic investigation of the dielectric properties in $\text{Ba}_{0.6}\text{Sr}_{0.4}\text{TiO}_3$ (BSTO) thin films grown on $0.29(\text{LaAlO}_3):0.35(\text{Sr}_2\text{TaAlO}_6)$ (LSAT) substrates as a function of film thickness. The evolution of the microstructure was carefully analyzed using a JEOL 4000 FX transmission electron microscope (TEM) operated at 300 keV as well as a Siemens D5000 four-circle x-ray diffractometer (XRD). The in-plane dielectric constant ϵ_{11} was mapped as a function of film thickness and by using a basic thermodynamic model we are able to correctly interpret its evolution. In addition, we show compelling evidence that local strain fields associated with threading dislocations in our films severely impact the dielectric response.

The BSTO films were fabricated using $1 \text{ cm}^2 \times 0.5 \text{ mm}$ LSAT substrates by pulsed-laser deposition (PLD). The substrate temperature was held at 800°C during deposition while a dynamic pressure of 120 mTorr O_2 was established in the chamber. A 248 nm laser with a fluence of $1.5\text{--}2 \text{ J/cm}^2$ was used, corresponding to a growth rate of 0.15 nm/s . Films were fabricated using $\text{Ba}_{0.6}\text{Sr}_{0.4}\text{TiO}_3$ high-density ceramic targets and ranged in thickness from 8 to 350 nm. The

dielectric measurements were performed by using the conventional interdigital electrode (IDE), consisting of 50 fingers separated by a $15 \mu\text{m}$ gap. Each finger had a width of a $25 \mu\text{m}$ finger and length of roughly 0.70 cm . Standard photolithography techniques were used to define the pattern and metallization performed via deposition of a 100 nm Au layer using PLD. The dielectric properties were then measured using an HP 4192 impedance/gain analyzer.

Standard $\theta\text{--}2\theta$ XRD scans revealed only $(00l)$ -type reflections and no evidence of second-phase nucleation in the BSTO layer for all of our films. The evolution of the out-of-plane lattice constant a^\perp is shown as a function of film thickness in Fig. 1 (closed squares). The thinnest films are under compressive in-plane stress ($\leq 0.25\%$), which is relaxed in a continuous fashion as the thickness increases. The open circles represent a theoretical calculation for a^\perp as a function of thickness. Based on the RT lattice parameters of the target and the substrate ($a_s = 0.38650 \text{ nm}$), we would expect com-

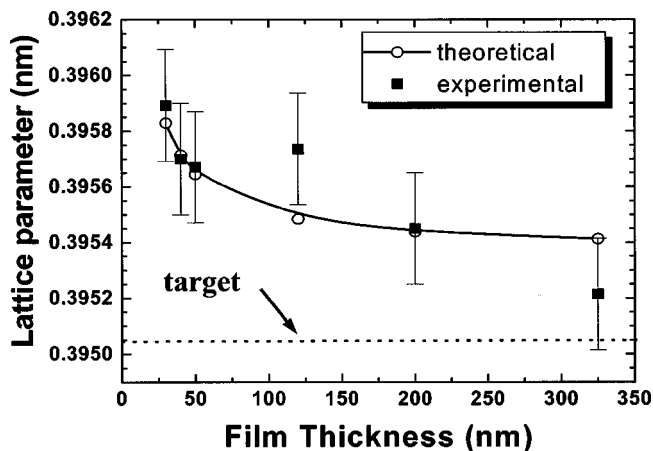


FIG. 1. Evolution of a^\perp as a function of film thickness. Also shown is the theoretical curve given by the open circles. The straight dashed line represents the lattice parameter of the ceramic target ($a^0 = 0.39505 \text{ nm}$).

^{a)}Electronic mail: haoli@glue.umd.edu

pressive in-plane stress within the film for all film thicknesses, as observed in our XRD analysis. The out-of-plane lattice parameter can be related to the in-plane strain x_M as follows:

$$x^\perp = \frac{a^\perp - a^0}{a^0} = -\frac{2C_{12}}{C_{11}}x_M = -\frac{2C_{12}}{C_{11}}\left(\frac{a_S - a^0}{a_S}\right), \quad (1)$$

where C_{ij} are elements of the elastic moduli at fixed polarization.¹² x_M for the thicker films (film thickness $h \geq 100$ nm) are an order of magnitude less than the lattice mismatch between the film and the substrate, i.e., $x_M^0 = (a_S - a^0)/a_S$ due to relaxation by misfit dislocation formation.

Assuming that no additional dislocations form during cooling down from T_G ,¹³ this relaxation can be taken into account using an ‘‘effective’’ substrate lattice parameter \bar{a}_S .^{14,15} The critical thickness for dislocation formation is around 2 nm for BSTO and LSAT, calculated from the Matthews–Blakeslee criteria.¹⁶ The degree of relief provided by misfit dislocations increases with thickness, which lowers the out-of-plane parameter towards its equilibrium value of 0.395 05 nm. The theoretical values of the out-of-plane lattice parameters were calculated replacing a_S in Eq. (1) with \bar{a}_S . They are in excellent agreement with the experimentally observed values. The thermal expansion coefficients of BSTO and LSAT were taken to be 10×10^{-6} and $11 \times 10^{-6} \text{ }^\circ\text{C}^{-1}$, respectively. Rocking-curve ω scans revealed peak widths of the BSTO (002) reflection of less than 0.15° , the resolution of the diffractometer. A similar investigation of [011] reveals a larger value of 0.05° indicating larger in-plane mosaic spread.

ϵ_{11} data as a function of voltage at 1 MHz for several samples within the thickness series is shown in Fig. 2(a). For thicker films the permittivity of the BSTO was extracted from the capacitance data using a model outlined by Gevorgian, Linner, and Kollberg.¹⁷ For the very thin films (≤ 50 nm), where the effect of the film on the overall capacitance is small, a perturbation approach was adopted. The contribution from the LSAT substrate to the capacitance was measured by depositing IDEs on several bare LSAT pieces. The value obtained was modified to account for the addition of the BSTO layer by using corrections obtained from the model mentioned previously.

As can be seen in Fig. 2(a), all BSTO films in this series display hysteresis in their C – V characteristics. From the literature for bulk BSTO(60:40), T_C is reported to occur at $\sim 2^\circ\text{C}$. Epitaxial strains or defects can cause shifts in T_C in the case of thin films,^{9,10,18} as observed for our films. We have extracted from the ϵ_{11}/ϵ_0 versus applied voltage curves the zero-field value and plotted it as a function of film thickness [Fig. 2(b)]. The dotted line suggests that the dielectric constant decreases rapidly with decreasing thicknesses below 100 nm. Also, ϵ_{11} saturates for the thicker films at a value (~ 1400) which is significantly lower than that measured on bulk BSTO (≥ 5000) at RT. The $\tan \delta$ is relatively insensitive to film thickness, fluctuating around a value of 0.035. In addition, the tuning characteristics follow a similar trend as the dielectric constant, saturating at a value slightly higher than 50% at 40 V.

It is reasonable to explain the decrease in the thin-film limit as a consequence of the compressive in-plane strain in

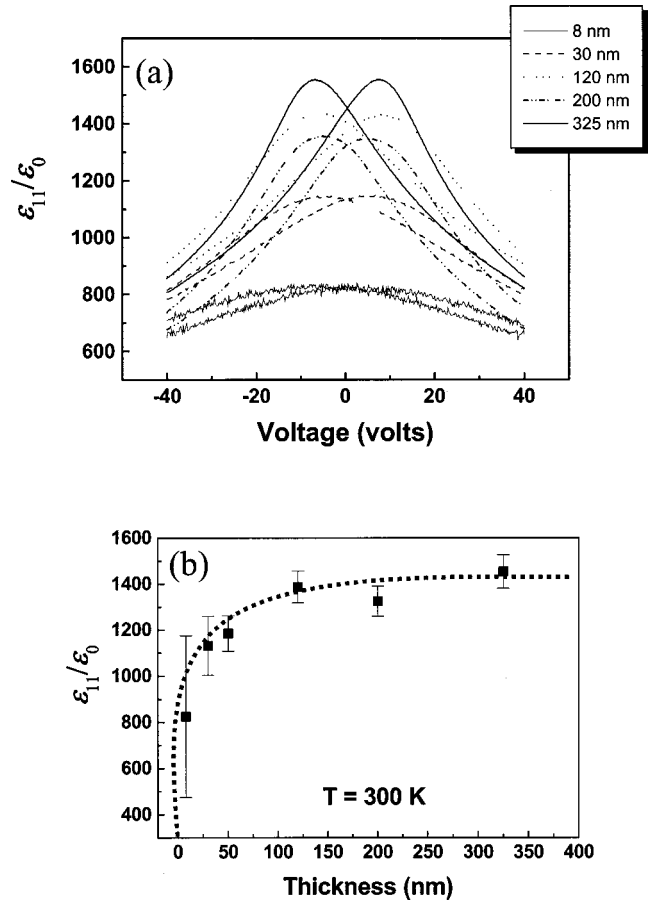


FIG. 2. (a) ϵ_{11}/ϵ_0 as a function of voltage for five films within the thickness series. (b) Evolution of ϵ_{11}/ϵ_0 as a function of film thickness. The dashed line is a guide for the eyes.

this regime. The dependence of the dielectric constant on internal stresses can be determined from

$$F(P) = \frac{1}{2}\alpha P^2 - PE + F_{el}(P), \quad (2)$$

where $\alpha = (T - T_C)/2\epsilon_0 C$ is the dielectric stiffness, T_C and C are the Curie temperature and constant, respectively, ϵ_0 is the permittivity of free space, P is the polarization induced by the electric field E along the [100] direction, and F_{el} is the elastic energy. The elastic energy is given in terms of the components of the stress and strain tensors σ_i and x_i (in the Voigt notation), respectively, as

$$F_{el} = \frac{1}{2}(\sigma_1 x_1 + \sigma_2 x_2), \quad (3)$$

since the mechanical boundary conditions require that $\sigma_3 = 0$ and $\sigma_4 = \sigma_5 = \sigma_6 = 0$ (no shear stresses). If there is no applied field, $F_{el} = \sigma x_M$ since $\sigma_1 = \sigma_2$ and $x_1 = x_2 = x_M$ where $x_M = (\bar{a}_S - a^0)/\bar{a}_S$ is the misfit strain. However, if there is an applied field $E \parallel [100]$, $x_1(P) = x_M + Q_{11}P^2$ and $x_2(P) = x_M + Q_{12}P^2$, where Q_{ij} are the electrostrictive coefficients. The relative dielectric constant is thus given by

$$\epsilon_r = \frac{\epsilon_{11}}{\epsilon_0} = \left(2\epsilon_0 \left. \frac{\partial^2 F}{\partial P^2} \right|_{P=0} \right)^{-1} = \frac{1}{2\epsilon_0[\alpha - \bar{C}x_M(Q_{11} + Q_{12})]}, \quad (4)$$

where $\bar{C} = C_{11} + C_{12} - 2C_{12}^2/C_{11}$. The dependence of the reciprocal dielectric constant on the misfit strain is illustrated in Fig. 3. For the electrostrictive coefficients of BSTO, we

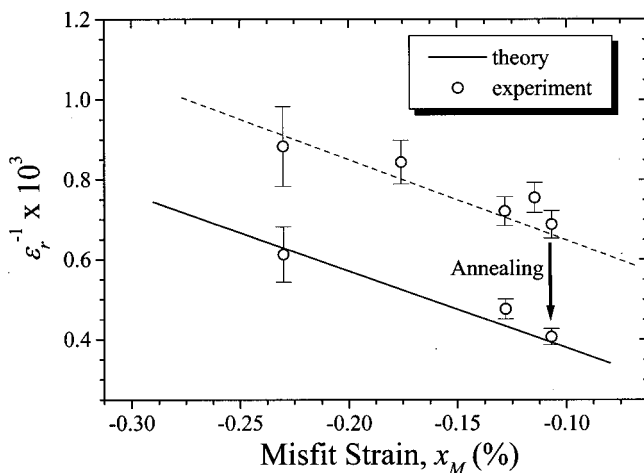


FIG. 3. Theoretical dependence of the reciprocal dielectric constant on the film thickness and the experimental data. The dashed line is the theoretical curve shifted upwards such that it fits the experimental data. The dielectric constant of the annealed samples are in good agreement with the theoretical prediction.

have taken typical values for perovskite oxides ($Q_{11} = 0.1 \text{ m}^4/\text{C}^2$ and $Q_{12} = -0.035 \text{ m}^4/\text{C}^2$). The dielectric stiffness at RT was determined to be $1.06 \times 10^7 \text{ m/F}$ by averaging the Curie constants of BaTiO_3 ($1.5 \times 10^5 \text{ }^\circ\text{C}$) and SrTiO_3 ($0.8 \times 10^5 \text{ }^\circ\text{C}$),^{19,20} and taking $T_C = 2 \text{ }^\circ\text{C}$.²¹ For stress-free films, the theoretical relative dielectric constant is approximately 5300, in good agreement with the bulk value at RT. Superimposed on Fig. 3 are the experimental values of the reciprocal dielectric constant and the corresponding misfit strain. For the experimental values, the same trend as the theoretical calculation is observed. However, the curve has shifted towards higher values, indicating a systematic decrease in the dielectric constant. We attribute the difference to the large threading dislocation density in our films. The dashed line is the theoretical estimation shifted upwards such that it fits the experimental observations. It suggests that the presence of the highly dense threading dislocation structure alters the dielectric stiffness of the material such that it results in an overall reduction in the dielectric constant. Upon annealing at $975 \text{ }^\circ\text{C}$ for 15 h, we observe a reduction in the threading dislocation density and a simultaneous recovery in the dielectric properties towards the theoretical estimate (the experimental points are marked on Fig. 3).

Plan-view bright-field TEM images of a 120 nm BSTO/LSAT film reveal a huge density of threading dislocations, with a density of $2.2 \times 10^{11} \text{ cm}^{-2}$, representing one threading dislocation within every 12.6 nm radius. This is 3–4 orders of magnitude higher than typically observed in semiconductors. All BSTO/LSAT films imaged for this work show similar threading dislocation densities.

High-resolution images reveal these dislocations to be edge type with a Burgers vector $\mathbf{b} = [100]_{\text{BSTO}}$. Associated with each dislocation is a local strain field which, in the vicinity of the core, is greater than the macroscopic misfit strain. Due to the extremely high densities measured for these films, it is quite likely that neighboring dislocations still have overlapping strain fields. Skulski and Wawrzala²²

have shown a broadening of the phase transition along with an overall decrease in dielectric constant as the density of these dislocations increases. The density we measure represents a five order increase over the values used in that work. These arguments strongly support local strain associated with threading dislocations as another mechanism for dielectric degradation in these heteroepitaxial BSTO thin films.

In summary, a series of heteroepitaxial BSTO thin films were prepared on LSAT substrates. The measured a^\perp values indicated the existence of compressive in-plane strain in these films which relaxed with increasing thickness, and represented only about 0.25% even for the thinnest sample. A theoretical model used to calculate the heteroepitaxial stresses in our films showed good agreement with the experimental measurements. A significant reduction of the dielectric constant was observed compared to bulk samples. TEM images suggest that local strain associated with a huge density of threading dislocations was responsible for this shift.

This work was partially supported by the NSF under Grant No. DMR-9903279, NSF-MRSEC under Grant No. DMR-96-32521, and an ARL-MRCP Agreement.

- ¹V. K. Varadan, D. K. Ghodgaonkar, V. V. Varadan, J. F. Kelly, and P. Glikerdas, *Microwave J.* **35**, 116 (1992).
- ²R. W. Babbitt, T. E. Kosciwa, and W. C. Drach, *Microwave J.* **35**, 63 (1992).
- ³L. Sengupta and S. Sengupta, *IEEE Trans. Ultrason. Ferroelectr. Freq. Control* **44**, 792 (1997).
- ⁴B. A. Baumert, L.-H. Chang, A. T. Matsuda, C. J. Tracy, N. G. Cave, R. B. Gregory, and P. L. Fejes, *J. Mater. Res.* **13**, 197 (1998).
- ⁵J. Im, O. Auciello, P. K. Baumann, S. K. Streiffer, D. Y. Kaufman, and A. R. Krauss, *Appl. Phys. Lett.* **76**, 625 (2000).
- ⁶F. W. Van Keuls, R. R. Romanofsky, N. D. Varaljay, F. A. Miranda, C. L. Canedy, S. Aggarwal, T. Venkatesan, and R. Ramesh, *Microwave Opt. Technol. Lett.* **20**, 53 (1999).
- ⁷M. D. Winters, C. H. Mueller, K. B. Bhasin, and F. A. Miranda, *Adv. Cryog. Eng.* **41**, 1747 (1996).
- ⁸D. Collier, *Integr. Ferroelectr.* **4**, 113 (1994).
- ⁹W. Chang, C. Gilmore, W. Kim, J. Pond, S. Kirchoefer, S. Qadri, D. Chrisey, and J. Horwitz, *J. Appl. Phys.* **87**, 3044 (2000).
- ¹⁰C. M. Carlson, T. V. Rivkin, P. A. Parilla, J. D. Perkins, D. S. Ginley, A. B. Kozyrev, V. N. Oshadchy, and A. S. Pavlov, *Appl. Phys. Lett.* **76**, 1920 (2000).
- ¹¹M. E. Lines and A. M. Glass, *Principles and Applications of Ferroelectrics and Related Materials* (Clarendon, Oxford, 1977).
- ¹²Since the elastic moduli are not given in the literature for single-crystal BSTO, we have used a simple averaging procedure based on the values for BaTiO_3 and SrTiO_3 . $C_{11}(\text{BaTiO}_3) = 2.75 \times 10^{11} \text{ N/m}^2$, $C_{12}(\text{BaTiO}_3) = 1.79 \times 10^{11} \text{ N/m}^2$, $C_{11}(\text{SrTiO}_3) = 3.48 \times 10^{11} \text{ N/m}^2$, and $C_{12}(\text{SrTiO}_3) = 1.00 \times 10^{11} \text{ N/m}^2$, from D. R. Lide, *Handbook of Chemistry and Physics*, 76th ed. (CRC, Boca Raton, FL, 1995), as cited in Ref. 9.
- ¹³S. P. Alpay, V. Nagarajan, L. A. Bendersky, M. D. Vaudin, S. Aggarwal, R. Ramesh, and A. L. Roytburd, *J. Appl. Phys.* **85**, 3271 (1999).
- ¹⁴J. S. Speck and W. Pompe, *J. Appl. Phys.* **76**, 466 (1994).
- ¹⁵S. P. Alpay and A. L. Roytburd, *J. Appl. Phys.* **83**, 4714 (1998).
- ¹⁶J. W. Matthews and A. E. Blakeslee, *J. Cryst. Growth* **27**, 118 (1974).
- ¹⁷S. S. Gevorgian, P. L. J. Linner, and E. L. Kollberg, *IEEE Trans. Microwave Theory Tech.* **44**, 896 (1996).
- ¹⁸C. L. Chen, H. H. Feng, Z. Zhang, A. Brazdeikis, Z. J. Huang, W. K. Chu, C. W. Chu, F. A. Miranda, F. W. Van Keuls, R. R. Romanofsky, and Y. Liou, *Appl. Phys. Lett.* **75**, 412 (1999).
- ¹⁹K. A. Müller and H. Burkhard, *Phys. Rev. B* **19**, 3593 (1979).
- ²⁰K. Uchino, S. Nomura, L. E. Cross, S. J. Jang, and R. E. Newnham, *J. Appl. Phys.* **51**, 1142 (1980).
- ²¹*Landolt-Börnstein, Numerical Data and Functional Relationships in Science and Technology*, Vol. 16, edited by K.-H. Hellwege and A. M. Hellwege (Springer, Berlin, 1981).
- ²²R. Skulski and P. Wawrzala, *Physica B* **233**, 173 (1996).